5. Improvement of LED Device Characteristics by Insertion of $Al_{0.06}Ga_{0.94}N/GaN$ SLS Cladding Underlayer

This chapter demonstrates fabrication and device evaluation of InGaN-based blue light emitting diode (LED) with insertion of $Al_{0.06}Ga_{0.94}N/GaN$ SLS cladding underlayer. A conventional blue LED grown on Si(111) substrate is also fabricated and evaluated for comparison, to demonstrate superior light emission characteristics and electrical characteristics that can be obtained by the insertion of $Al_{0.06}Ga_{0.94}N/GaN$ SLS cladding underlayer.

5.1 Introduction

Si(111) is a very promising substrate for the growth of low-cost GaN-based energy-saving light-emitting devices with wavelength ranging from ultra-violet to infrared illumination. However, large thermal mismatch of 116% and lattice mismatch of 17% between GaN epitaxial layer and the Si(111) substrate contribute to low-quality film with threading dislocation density (TDD) of approximately larger than $\sim 10^{10}$ (cm^{-2}) in conventional metal organic chemical vapor deposition (MOCVD) growth method [1]. The smaller band-gap of Si substrate compared to the band-gap of InGaN-based active layer in visible light-emitting device structure attributes to the absorption of emitted light by the substrate, causing poor light emission from the device. Ishikawa *et al.* have reported an improved light output power for light-emitting diode (LED) grown on Si(111) substrate using an $Al_{0.3}Ga_{0.7}N/AlN$ distributed Bragg reflector

(DBR) to reduce the optical loss [2]. However, the pair number is limited to 5 to obtain a crack-free film. In chapter 4, the author has reported reduction of TDD and enhancement of internal quantum efficiency (η_{iqe}) in InGaN-based multi-quantum well (MQW) with the insertion of $Al_{0.06}Ga_{0.94}N/GaN$ SLS cladding layer under the active layer [3]. The $Al_{0.06}Ga_{0.94}N/GaN$ SLS cladding layer can also be used to reduce optical loss to the substrate in LED operation. This chapter reports material characterization and fabrication of InGaN-based blue LED with $Al_{0.06}Ga_{0.94}N/GaN$ SLS cladding underlayer grown on Si(111) substrate. This study is intended to demonstrate the superior optical and electrical characteristics that can be achieved by the insertion of $Al_{0.06}Ga_{0.94}N/GaN$ SLS cladding underlayer in LED structure grown on Si(111) substrate.

5.2 Experimental Methods

The LED structure in this study was grown on 2 inches Si(111) substrate by horizontal-reactor MOCVD. Trimethylgallium (TMGa), trimethylaluminum (TMAl) and ammonia (NH_3) were used as precursors for Ga, Al and N, respectively. Hydrogen (H_2) was used as carrier gas. Monosilane (SiH_4) diluted in hydrogen was used for n-type dopant. The substrate was thermally cleaned at 1100°C in H_2 flow before growth. Prior to the growth of LED layers, a 20 nm thin high-temperature AlN layer was grown on the substrate as seeding-layer, followed by 40 pairs of AlN/GaN multilayer (ML) with respective thickness of 5 nm and 20 nm. Subsequently, a 400 nm thick $Al_{0.06}Ga_{0.94}N/GaN$ SLS cladding layer with respective thickness of 2.5 nm each was grown on the MLs. The growth was continued with 200 nm thick n^+-GaN contact layer,

active layer consisting of 15 pairs of 2 nm thick $In_{0.16}Ga_{0.84}N$ wells and 9 nm thick $In_{0.08}Ga_{0.92}N$ barrier layers, a 10 nm thick p-$Al_{0.08}Ga_{0.92}N$ electron-block layer, and a 50 nm thick p-GaN contact layer for the LED structure. A conventional sample grown with the same parameter but without the $Al_{0.06}Ga_{0.94}N$/GaN SLS cladding layer was also prepared for comparison. The layer structure of the LED is shown in Fig. 1.

Crystal properties of the samples were evaluated by Philips X'Pert Pro x-ray diffraction (XRD) system using hybrid double-axis diffractometer. Photoluminescence (PL) mapping was performed at room-temperature (RT) to evaluate the emission characteristics of the samples. The samples were fabricated into LED using standard device processing method reported elsewhere with Ni/Au semi-transparent electrode, Ni/Au p-type contact electrode, Ti/Al/Ni/Au top n-type contact electrode on the n^+-GaN contact layer and AuSb/Au backside n-type contact electrode on the n^+-type Si substrate [4]. Optical characteristics were measured at RT using an integrated sphere and electrical characteristics were measured using a standard semiconductor parameter analyzer.

5.3 Results and Discussions

All samples in this study are crack-free, showing specular surface and free from melt-back etching. Crystal quality is evaluated by x-ray rocking curve (XRC) ω scan of GaN, with symmetric (0004) scan associated with screw and mixed dislocations, while asymmetric $(20\bar{2}4)$ scan is associated with edge and mixed dislocations. The XRC properties of the samples in this study are shown in Table V.I. The full-width at half-maximum (FWHM) results in our samples are relatively larger

than results reported elsewhere by other groups due to the thin existence of pure GaN film in our structure. However, the comparison between samples in this study shows obvious improvement in crystal quality when SLS cladding layer is inserted in the structure. The (0004) scan result indicates that a lower density of screw dislocations can be obtained by the insertion of $Al_{0.06}Ga_{0.94}N$/GaN SLS underlying cladding layer. The result also indicates a small improvement of edge dislocation density in the structure.

Photoluminescence (PL) peak wavelength mapping is shown in Fig. 5.2, with (a) for sample with underlying $Al_{0.06}Ga_{0.94}N$/GaN SLS cladding layer, and (b) for conventional sample without the $Al_{0.06}Ga_{0.94}N$/GaN SLS cladding layer. Average MQW peak wavelength in (a) is 437.8 nm, and (b) is 471.9 nm. The $Al_{0.06}Ga_{0.94}N$/GaN SLS cladding layer reduces MQW wavelength peak fluctuations, with standard deviation value of 5.3% in (a) compared to 7.6% in (b). This result indicates that the $Al_{0.06}Ga_{0.94}N$/GaN SLS cladding layer is also effective to improve MQW wavelength peak uniformity.

Fig. 5.3 shows light intensity vs. current (*I-L*) characteristics for the samples. The results clearly show that LED structure with underlying $Al_{0.06}Ga_{0.94}N$/GaN SLS cladding layer yields a higher intensity and a higher saturation current compared to the conventional structure. At 50 mA current injection, the light intensity from LED with underlying $Al_{0.06}Ga_{0.94}N$/GaN SLS cladding layer is 34% higher than that of from conventional LED structure. In both structures, current injection from the top p-GaN contact layer to the backside n^+-type Si substrate shows a higher saturation current due to a better current spreading by the substrate, which also spreads heat uniformly in the LED chip.

Electroluminescence (EL) characteristics of the samples are shown in Fig. 5.4. The LED structure with underlying $Al_{0.06}Ga_{0.94}N$/GaN SLS cladding layer in (a) shows a narrower spectrum full-width at half maximum (FWHM) peak of 27 nm compared to that of 35 nm in conventional sample shown in (b). The narrower FWHM in sample with $Al_{0.06}Ga_{0.94}N$/GaN SLS cladding layer agrees well with the lower standard deviation result in PL wavelength peak mapping shown in Fig. 5.2, suggesting a uniform distribution of In composition can be achieved in the InGaN-based MQW by the SLS underlayer. The narrower FWHM is also attributed by superior crystal quality in the sample with $Al_{0.06}Ga_{0.94}N$/GaN SLS cladding underlayer compared to that of conventional LED structure, as discussed earlier.

The forward-bias current-voltage (*I-V*) characteristics are shown in Fig. 5.5. A tremendous improvement is seen in top-to-top (TT) *I-V* characteristics for sample with underlying $Al_{0.06}Ga_{0.94}N$/GaN SLS cladding layer, with operating voltage of 3.2 V at 20 mA current and series resistance of 16 Ω. This significant improvement is suggested due to a lower TDD in the sample, as described in chapter 4. The top-to-bottom (TB) *I-V* characteristics of the same sample shows higher operating voltage of 3.6 V at 20 mA and series resistance of 29 Ω, which is influenced by the highly resistive AlN/GaN ML in the buffer layer. The conventional structure shows almost similar characteristics as InGaN-based LED grown on AlN/sapphire template reported by our group elsewhere [5].

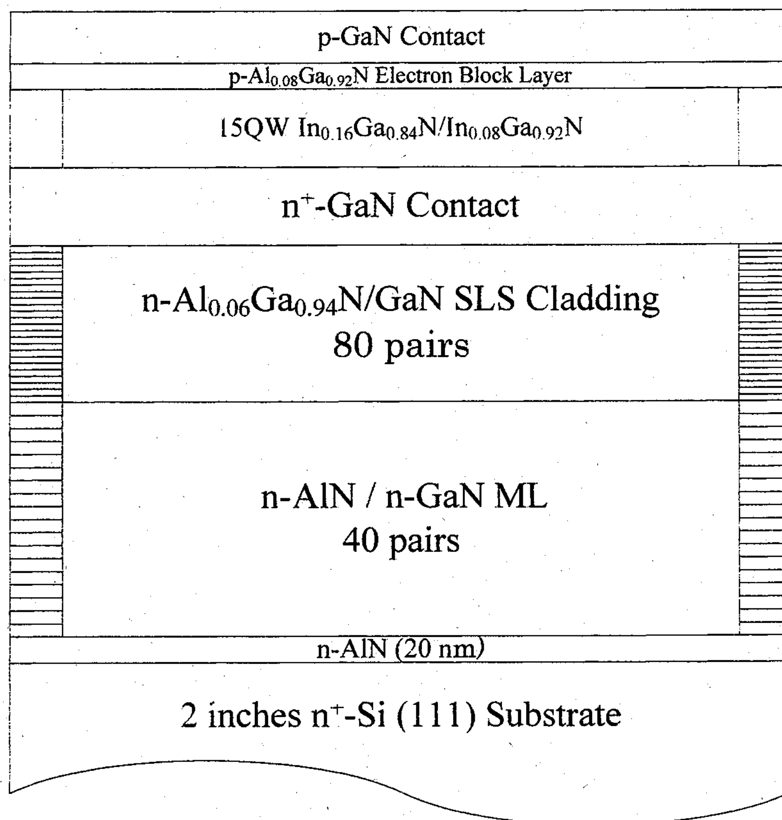

Fig. 5.1. LED structure grown on Si (111) substrate with underlying $Al_{0.06}Ga_{0.94}N/GaN$ SLS cladding layer.

Table V.I. XRC properties in LED structures with and without underlying SLS.

LED Sample		FWHM (arcsec)	Intensity (a. u.)
With $Al_{0.06}Ga_{0.94}N/GaN$ SLS	(0004)	884.8	28400.3
	$(20\bar{2}4)$	1826.2	563.8
Without $Al_{0.06}Ga_{0.94}N/GaN$ SLS	(0004)	1178.4	7498.6
	$(20\bar{2}4)$	1889.7	332.7

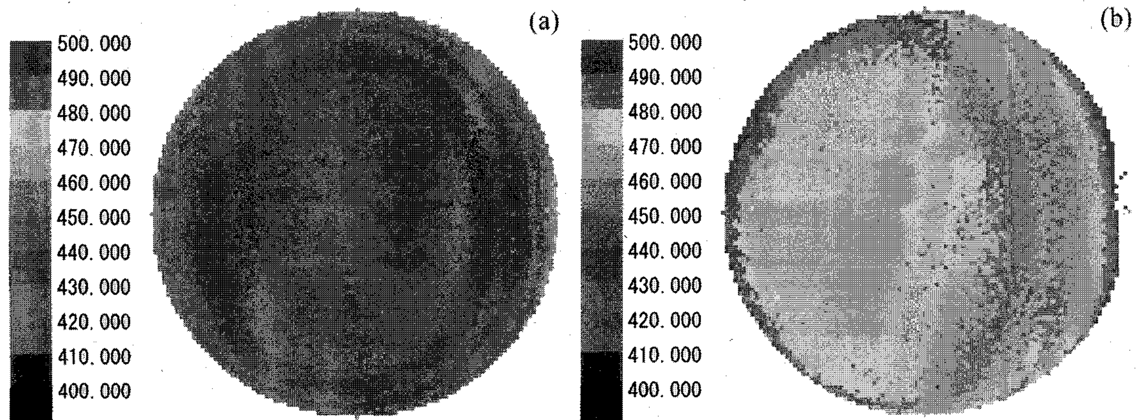

Fig. 5.2. PL wavelength peak mapping for LED structure of (a) with underlying $Al_{0.06}Ga_{0.94}N$/GaN SLS cladding layer and (b) conventional sample. Standard deviation in (a) is 5.3%, and (b) is 7.6%.

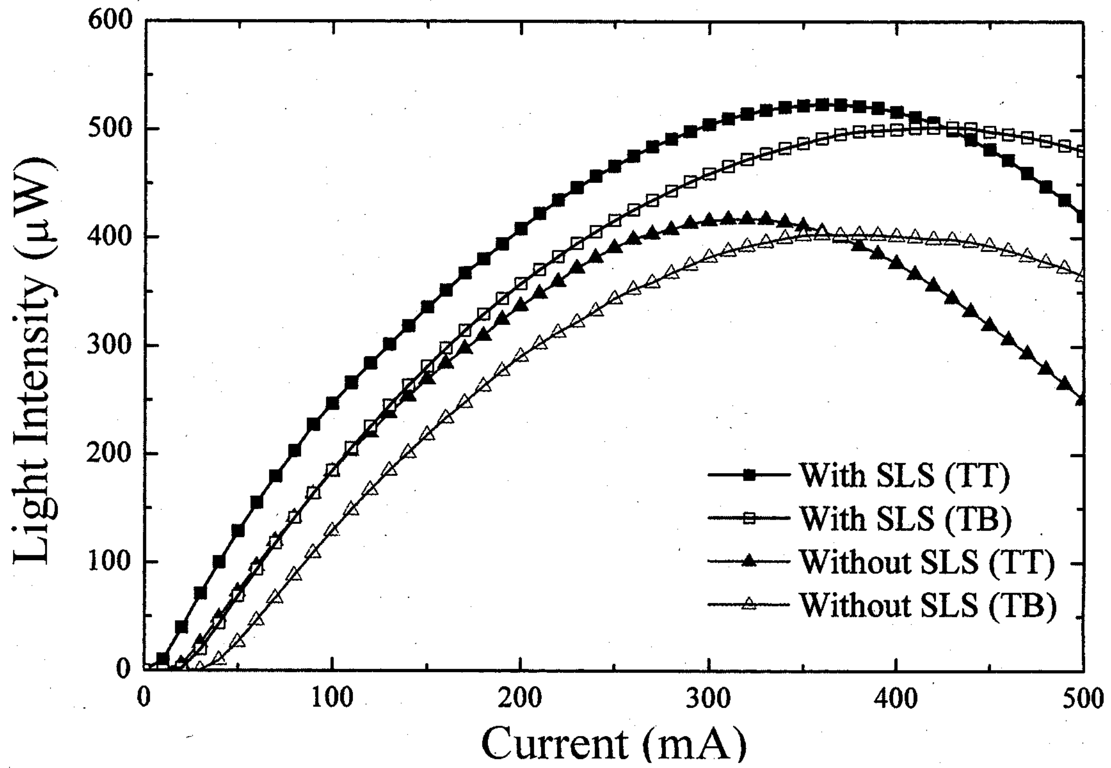

Fig. 5.3. Light intensity vs. current (*I-L*) characteristics for LED with underlying $Al_{0.06}Ga_{0.94}N$/GaN SLS cladding layer and conventional sample. (TT indicates current injection from top p-GaN to top n^+-GaN layer, while TB indicates current injection from top p-GaN to backside n^+-type Si substrate).

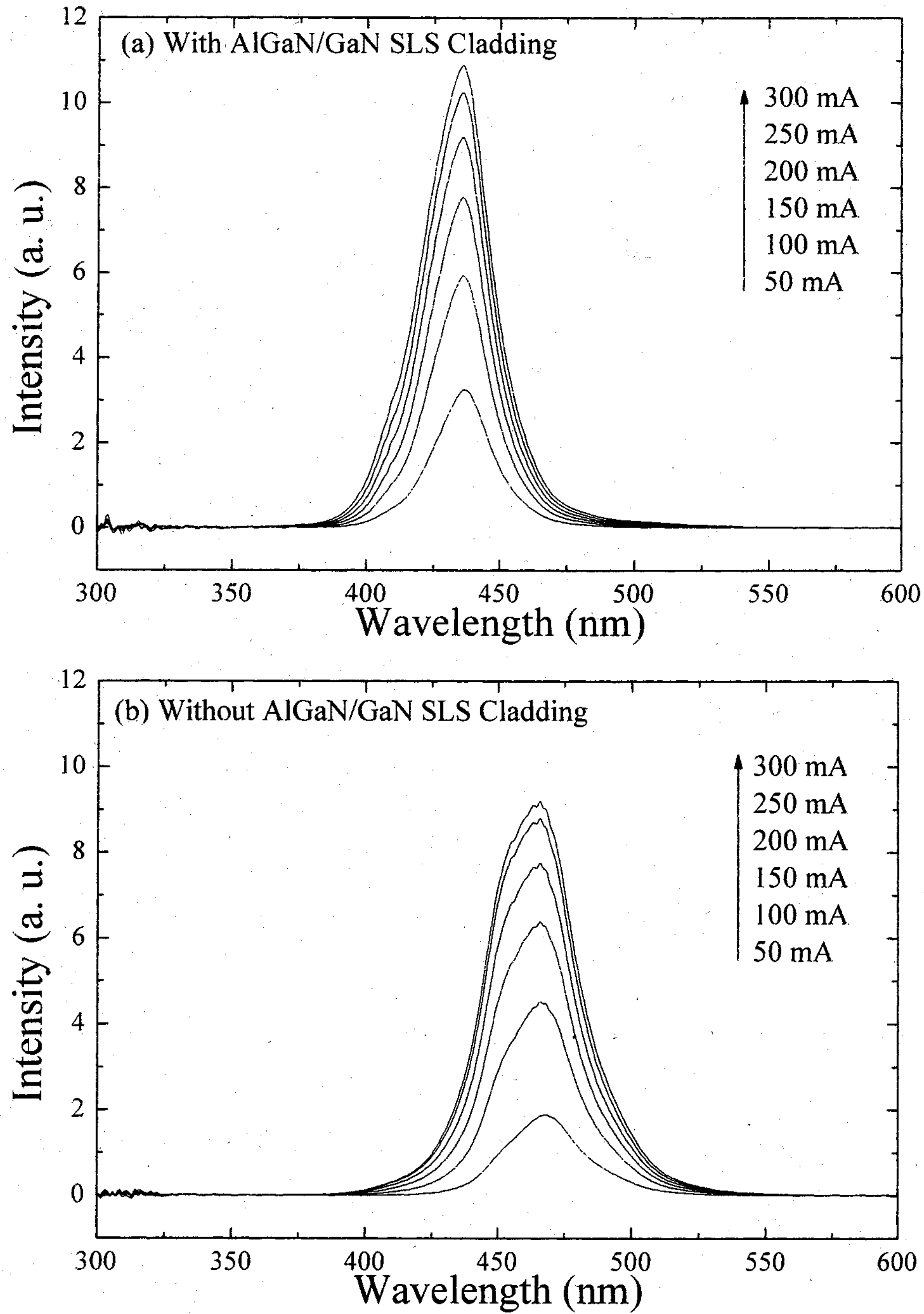

Fig. 5.4. EL characteristics for LED (a) with underlying $Al_{0.06}Ga_{0.94}N/GaN$ SLS cladding and (b) for conventional sample.

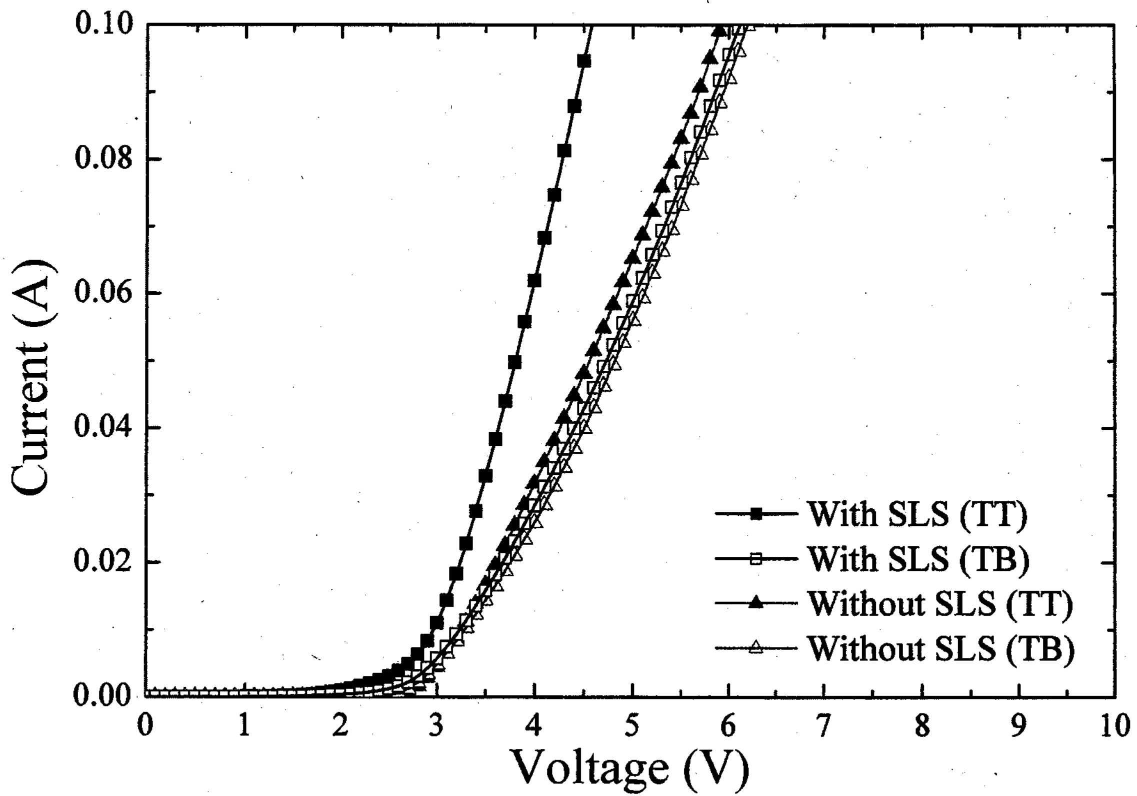

Fig. 5.5. Current vs. voltage (*I-V*) characteristics for LED with underlying $Al_{0.06}Ga_{0.94}N$/GaN SLS cladding layer and conventional sample. (TT indicates current injection from top p-GaN to top n^+-GaN layer, while TB indicates current injection from top p-GaN to backside n^+-type Si substrate).

5.4 Conclusions

This study shows that the insertion of $Al_{0.06}Ga_{0.94}N$/GaN SLS cladding layer with a low composition of Al under the active layer is effective to improve crystal quality, improve MQW wavelength peak uniformity, and improve overall optical and electrical characteristics in blue LED grown on Si(111) substrate. Light reflectance from the underlying cladding layer has also improved the LED optical characteristics with a higher light intensity and a narrower FWHM spectrum.

References

[1] T. Egawa, B. Zhang, N. Nishikawa, H. Ishikawa, T. Jimbo and M. Umeno, J. Appl. Phys. **91**, 528 (2002).

[2] H. Ishikawa, K. Asano, B. Zhang, T. Egawa and T. Jimbo, Phys. Stat. Sol. A **201**, 2653 (2004).

[3] B. A. B. Ahmad Shuhaimi, T. Suzue, Y. Nomura, Y. Maki and T. Egawa, Mater. Res. Soc. Symp. Proc. **1167**, O02-05 (2009).

[4] B. J. Zhang, T. Egawa, H. Ishikawa, N. Nishikawa, T. Jimbo and M. Umeno, Phys. Stat. Sol. A **188**, 151 (2001).

[5] B. Zhang, T. Egawa, Y. Liu, H. Ishikawa and T. Jimbo, Phys. Stat. Sol. C **0**, 2244 (2003).

6. Summary

This dissertation describes the research on material characterization, fabrication and evaluation for GaN-based light emitting devices grown on Si(111) substrate. Epitaxial growth of GaN on Si(111) has serious problems of substrate bowing and high threading dislocation density exceeding 10^{10} cm^{-2}, resulted by 116% thermal expansion coefficient difference and 17% lattice mismatch between GaN and Si(111). The high threading dislocation density (TDD) is the major obstacle to realize high performance GaN-based light emitting devices on Si(111) substrate. For instance, the high TDD quickly degrades device lifetime which is critical for application in commercial products. Large substrate bowing is also the origin of cracks in the epitaxial layer, limiting the total epitaxial growth thickness to less than 2 μm in this study to obtain crack free layer.

Our group utilizes AlN nucleation layer and AlN/GaN multilayer (ML) prior to the growth of layers for GaN-based devices. In normal growth design for LED, n-type electrode layer, active layer, and p-type electrode layer is followed after the AlN/GaN ML layer. In this conventional design, light emitted from MQW in the active layer is absorbed by the underlying Si(111) substrate.

In our approach to improve total material, optical and electrical characteristics of GaN-based devices on Si(111) substrate, we have introduced $Al_{0.06}Ga_{0.94}N$/GaN SLS cladding layer prior to the growth of InGaN-based MQW active layer. In chapter 4, the effect of the $Al_{0.06}Ga_{0.94}N$/GaN SLS cladding layer was investigated, in comparison with normal bulk $Al_{0.03}Ga_{0.97}N$ cladding layer in section 4.1, and in comparison with conventional GaN underlayer in section 4.2. It was found that in sample with

$Al_{0.06}Ga_{0.94}N$/GaN SLS cladding layer, threading dislocations (TDs) surpassing the interface between AlN/GaN ML and $Al_{0.06}Ga_{0.94}N$/GaN SLS radically disappear at the lower region in the $Al_{0.06}Ga_{0.94}N$/GaN SLS cladding layer. TDs that surpass the interface bend abruptly and annihilate in the $Al_{0.06}Ga_{0.94}N$/GaN SLS cladding layer. Furthermore, no formation of new TD is found at the interface between AlGaN/GaN ML and $Al_{0.06}Ga_{0.94}N$/GaN SLS. This characteristics has resulted in reduction of TDD in sample with $Al_{0.06}Ga_{0.94}N$/GaN SLS cladding layer, and significantly improves internal quantum efficiency (η_{iqe}) to 31.6% when the MQW thickness is reduced to 2 nm.

Further investigation on MQW emission mechanism and strain characteristics for sample with $Al_{0.06}Ga_{0.94}N$/GaN SLS cladding layer is described in section 4.2. Samples with 10 pairs of InGaN-based MQW were grown with $Al_{0.06}Ga_{0.94}N$/GaN SLS cladding underlayer, and conventional GaN underlayer. Varshni thermal coefficient analysis applied to each of the sample indicates that emission in both samples is contributed by delocalized excitons at low temperature until 50 K, and localized excitons give stronger contribution to the MQW emission when temperature is increased beyond 50 K. Sample with $Al_{0.06}Ga_{0.94}N$/GaN SLS cladding underlayer shows smaller emission peak shift than that of conventional GaN underlayer.

Arrhenius fittings in sample with $Al_{0.06}Ga_{0.94}N$/GaN SLS cladding underlayer suggest that the quenching of the luminescence with temperature is attributed by non-radiative recombination centers in the InGaN MQW, and thermal escape of electrons and/or holes from InGaN wells into InGaN barriers. Meanwhile, in sample with conventional GaN underlayer, thermal quenching is attributed by non-radiative recombination centers in the InGaN MQW, and thermal escape of electrons and/or holes from localized states and/or capture at non-radiative recombination centers in InGaN

wells.

Internal quantum efficiency (η_{iqe}) is estimated to be 29.4% in sample with $Al_{0.06}Ga_{0.94}N/GaN$ SLS underlayer, relative to only 20.6% in conventional GaN underlayer. TD inclination is observed in TEM dark-field image for sample with $Al_{0.06}Ga_{0.94}N/GaN$ underlayer, similar to sample in section 4.1, which improves TDD in the sample, which is the reason for η_{iqe} enhancement.

In understanding why the TD inclination occurs in sample with $Al_{0.06}Ga_{0.94}N/GaN$ SLS cladding underlayer, reciprocal space mapping (RSM) around $(10\bar{1}5)$ diffraction plane was measured in the samples. The result indicates that in-plane GaN lattice constant in sample with $Al_{0.06}Ga_{0.94}N/GaN$ SLS underlayer is compressive, relative to GaN lattice constant in conventional GaN underlayer. The compressive GaN layer in $Al_{0.06}Ga_{0.94}N/GaN$ SLS pair is suggested to force TD lines in the sample to bend abruptly, thus reducing TDD in the sample. The lower TDD subsequently reduces non-radiative recombination centers in the InGaN MQW and simultaneously increases η_{iqe} of the InGaN MQW.

Improvement in optical characteristics is also proven when AlGaN/GaN SLS cladding layer is used as opposed to AlGaN-based bulk cladding layer in laser diode (LD) structure grown on Si(111) as demonstrated in section 4.3.

Enhancement of optical and electrical characteristics from the insertion of $Al_{0.06}Ga_{0.94}N/GaN$ SLS is demonstrated in LED device fabrication and evaluation described in chapter 5. LED structure grown with $Al_{0.06}Ga_{0.94}N/GaN$ SLS cladding layer was compared with a conventional LED structure without any cladding layer on Si(111) substrate. The insertion of $Al_{0.06}Ga_{0.94}N/GaN$ SLS underlayer has shown to improve epitaxial layer quality in x-ray diffraction (XRD) analysis, improve wavelength peak

uniformity in photoluminescence (PL) surface mapping, and improve optical and electrical characteristics in the LED sample. A 34% increase of light intensity at 50 mA current injection and a narrower electroluminescence (EL) peak have been achieved by the insertion of $Al_{0.06}Ga_{0.94}N$/GaN SLS cladding underlayer. LED with $Al_{0.06}Ga_{0.94}N$/GaN underlayer also shows superior current-voltage (*I-V*) characteristics with operation voltage of 3.2 V at 20 mA and series resistance of 16 Ω.

Scope for Future Work

In this dissertation, the material and device improvement is limited to GaN epitaxy on Si(111) which utilizes AlN nucleation layer and AlN/GaN ML. Even though the insertion of $Al_{0.06}Ga_{0.94}N$/GaN SLS cladding underlayer improves the overall material quality, optical and electrical characteristics in the investigated epitaxial structure and device, there are wide possibility for further quality and performance improvement by combining with other methods, such as Si_xN_{1-x} interlayer, etc. There are also other advance methods for epitaxial quality improvements, such as, i) epitaxial lateral overgrowth (ELO), ii) pendeo epitaxial overgrowth (PEO), etc., which is not yet widely investigated for III-V nitride growth on Si substrate. The said methods are thought to significantly reduce TDD in the epitaxial layer, resulting in a high performance and reliable device lifetime. The author believes that the advance growth techniques such as ELO or PEO, are the necessary techniques that must be performed to achieve a commercial-grade high-performance III-V nitride-based HB-LED and LD on Si substrate.